International Journal of Chemical, Materials and Biomolecular Sciences
ISSN: 2415-6620
Vol:14, No:12, 2020

Characterization of a Hypoeutectic Al Alloy Obtained by Selective Laser Melting

Jairo A. Muñoz, Alexander Komissarov, Alexander Gromov

***Abstract*—**In this investigation, a hypoeutectic AlSi11Cu alloy was printed. This alloy was obtained in powder form with an average particle size of 40 µm. Bars 20 mm in diameter and 100 mm in length were printed with the building direction parallel to the bars' longitudinal direction. The microstructural characterization demonstrated an Al matrix surrounded by a Si network forming a coral-like pattern. The microstructure of the alloy showed a heterogeneous behavior with a mixture of columnar and equiaxed grains. Likewise, the texture indicated that the columnar grains were preferentially oriented towards the building direction, while the equiaxed followed a texture dominated by the cube component. On the other hand, the as-printed material strength showed higher values than those obtained in the same alloy using conventional processes such as casting. In addition, strength and ductility differences were found in the printed material, depending on the measurement direction. The highest values were obtained in the radial direction (565 MPa maximum strength and 4.8% elongation to failure). The lowest values corresponded to the transverse direction (508 MPa maximum strength and 3.2 elongation to failure), which corroborate the material anisotropy.

***Keywords*—**Additive manufacturing, aluminium alloy, melting pools, tensile test.

I. Introduction

NOWADAYS, additive manufacturing (AM) technologies prove to be the revolution in terms of new materials processing with structural applications [1]-[3]. This fact is attributed to greater flexibility and speed of production, reduced amount of wasted material, and a low number of manufacturing steps delivering a nearly finished product after printing [4]-[6]. The selective laser melting (SLM) process stands out within the wide variety of AM techniques. In this process, the pieces are obtained by melting and re-melting consecutive powder layers until the piece is final shaped without the need for a mold [7], [8]. However, there are also problems associated with the processing of metallic materials with AM techniques [9], [10]. Some of the issues are related to the materials' properties to be processed, such as the high reflectivity of aluminum that causes high powers to be needed to melt the powders forming pores [11]. It has also been shown that alloying elements such as copper, magnesium, zinc, among others, can cause the formation of microcracks because they promote large regions of solidification [12], [13]. For this reason, Al-Si alloys, which are characterized by their good mechanical properties, and their short solidification ranges, have attracted attention [14], [15]. Another of the most common problems is the growth of columnar grains [16], [17] caused by the thermal gradients involved in AM processes such as SLM due to the fusion and refusion of new layers on the already solidified layers. In this way, the directional growth of grains generates anisotropy in printed materials, one of the most critical research topics in the scientific community [18]-[20]. To better understand these phenomena, it is necessary to know the materials' microstructural characteristics and the relationship with their mechanical response. Therefore, this manuscript aims to study the microstructure of an AlSi11Cu alloy and its relationship with tensile mechanical properties. Different microstructural characterization techniques such as optical microscopy (OM), scanning electron microscopy (SEM), electron back-scattering diffraction (EBSD) were used to achieve the objective. Furthermore, the microstructure results were correlated with uniaxial tensile tests in different directions concerning the building direction (BD).

Jairo A. Muñoz is with National University of Science and Technology "MISIS", Moscow 119049, Russia (phone: +79161624057; e-mail: munos.bk@misis.ru).

Alexander. Komissarov is with National University of Science and Technology "MISIS", Moscow 119049, Russia (phone: +79168346634; e-mail: komissarov.alex@gmail.com).

Alexander. Gromov is with National University of Science and Technology "MISIS", Moscow 119049, Russia (phone: +79859322556; e-mail: alexandergromov1@gmail.com).

II. Materials and Methods

A. Initial Material

Fig. 1 (a) indicates the material received in powder form with an average particle size of 40 µm (D_{10} 19.6 µm, D_{50} 40.4 µm, and D_{90} 58.6 µm). Table I indicates the chemical composition of the alloy.

TABLE I
Chemical Composition of the Alloy

Element	Mg	Si	Ti	Mn	Fe	Cu	Al
wt %	0.54	10.73	0.22	0.49	0.25	0.72	Balance

B. Printed Material

The material was printed by SLM in a controlled Argon atmosphere using a SLM280HL printer with the following operating parameters: scan speed of 1650 mm/s, power of 370 W, and Hatch spacing of 130 µm (see Fig. 1 (b)).

C. Microstructure Characterization

Initially, the microstructure of the printed material was studied by OM using a Zeiss AX10 microscope. Keller's reagent (2.5% HNO_3, 1% HF, 1.5% HCl, and 95% distilled water) was used to reveal the microstructure. Microstructural characteristics were analyzed using ImageJ software. For greater detail of the microstructure, a SEM TESCAN VEGA

SBH3 from Oxford Instruments was used. Using EBSD, different microstructure characteristics, such as grain size, misorientations, and texture, were quantified.

The EBSD samples were analyzed with the following procedure: the material's surface was polished from a 2500 sandpaper passing through 9 µm, 3 µm, and 1 µm diamond suspensions and ending with colloidal silica with a particle size of 400 nm. Subsequently, the polished surface was electropolished at 20 kV for 15 s (electrolyte of 30% glycerin, 20% HCl, and alcohol).

D.Mechanical Properties

The material's tensile strength was assessed by uniaxial tests at room temperature with a constant strain rate of 1×10^{-3} s^{-1}. Bone-shaped samples with gauge dimensions of 4 mm × 1.3 mm × 2 mm were cut in different directions (see Fig. 1 (c)). Through digital image correlation (DIC), the deformation of the tensile tests was quantified.

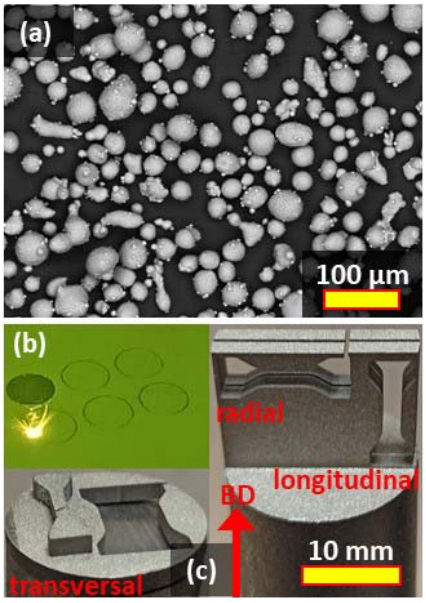

Fig. 1 (a) Powder particles, (b) SLM processing, and (c) as-printed material and tensile samples orientation

III. Results and Discussion

A. As-printed Material

Fig. 2 (a) shows the printed alloy's microstructure with the BD parallel to the bars' longitudinal direction. This figure indicates the formation of stacked cylindrical-shaped melting pools (MP). Looking in detail within the MP, Fig. 2 (b) highlights the presence of two phases differentiated by their light and dark colors. In this case, according to [21], corresponding to the Al matrix (light color), which is surrounded by an interconnected network rich in Si (dark color). In Fig. 2 (b), the presence of a melting pool boundary (MPB) is also highlighted by the dashed red lines. It is appreciated that within the MPB, there is a larger expansion of the Si network. In contrast, within the MP, the Al matrix and the Si network form a more homogeneously distributed pattern. This behavior can be attributed to fusion and refusion between layers that give rise to high thermal impact areas during printing the material [22]. Using energy-dispersive X-ray spectroscopy (EDX), it can be evaluated that the areas presented dark by OM and light by SEM correspond to areas enriched in Si, according to the EDX spectrum in Fig. 2 (c). Therefore, it is clear that the printed alloy is made up of Al's matrix and a network enriched in Si. In addition, it is also shown that the MPBs are regions where there is considerable distortion of the Si-rich network due to the more significant thermal gradients that occur in these areas.

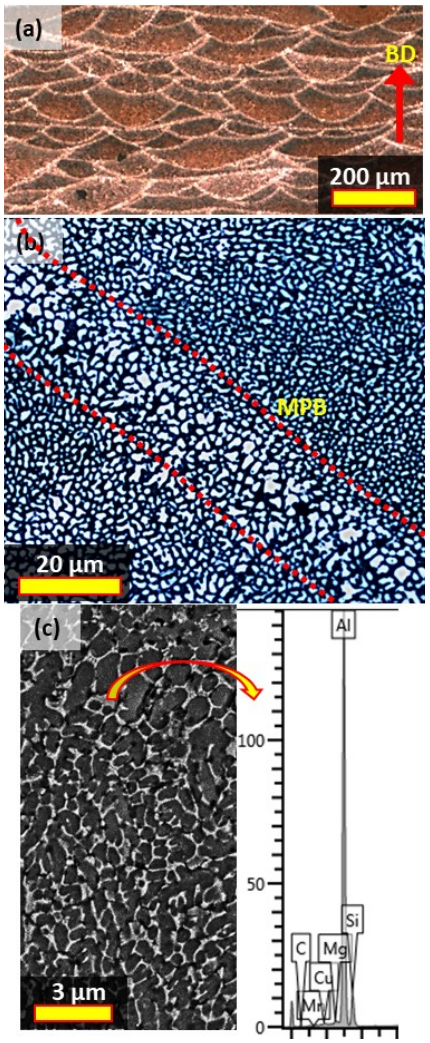

Fig. 2 (a) As-printed material optical micrographic, (b) microstructure inside two MPs, and (c) EDX spectra

To better understand the microstructure's characteristics, Figs. 3 (a) and (b) indicate the distributions corresponding to the Al matrix and the Si-enriched network, respectively. Using ImageJ, the zones corresponding to the matrix and the Si-rich phase can be clearly separated by selecting a suitable value of each phase's color threshold. Therefore, Fig. 3 (a) shows that

the Al cell size has a mean value of 0.95 µm occupying an area of 34%. On the other hand, Fig. 3 (b) reveals that the Si network also follows a logarithmic normal distribution with a mean value of 0.9 µm occupying 66% of the area.

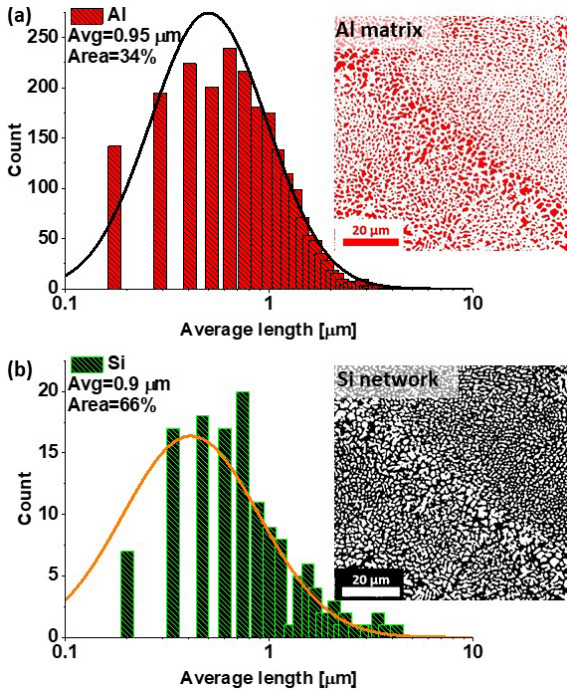

Fig. 3 (a) Al matrix size and (b) Si network distribution

B. Microstructure Characterization

Fig. 4 summarizes the microstructural properties quantified by EBSD. Fig. 4 (a) shows the inverse pole figure (IPF) map in the BD. At first glance, this map allows observing the existence of a combination of equiaxed grains and others elongated towards the BD. Furthermore, it is appreciated that there is a preferential texture towards the direction <001> ∥BD, especially from the elongated grains. In contrast, equiaxed and smaller grains appear to follow the <111> direction. These observations allow visualizing that AM processes such as SLM induce a heterogeneous state in the material.

Fig. 4 (b) shows the grain size distribution as a function of the area fraction with a mean grain size of 9.9 µm. From this figure, it is also possible to evaluate and confirm the existence of two families of grain size, the one formed by grain sizes smaller than 10 µm and occupying 33% of the area, and the other family with sizes bigger than 10 µm occupying 67% of the area.

This observation is in agreement with [23], who also found a high fraction of columnar grains after printing an Al alloy. Therefore, it can be established that this behavior corresponds well with recrystallization and grain growth phenomena due to continuous temperature changes during the union of new layers [24]. Thus, misorientation angles distribution in Fig. 4 (c) indicates that the nature of the grain boundaries corresponds mainly to high-angle grain boundaries (HAGB). This distribution describes a behavior close to random with a HAGB fraction close to 90% and a mean misorientation of 33°. The low fraction of low-angle grain boundaries (LAGB) also reflects that the vast majority of grains have low distortions and that there is no high density of mobile dislocations within them.

C. Texture Evolution

To better understand the microstructural evolution of the printed material, through Fig. 5, the evolution of grain size and texture is analyzed, taking into account the grains' morphology. I.e., grain sizes with equiaxial and columnar morphology. With Figs. 5 (a) and (b), it is verified that the great majority of columnar (mostly, the largest grains) and equiaxed (mostly, the smallest grains) grains follow well-defined textures.

Separating the two populations of grains, Fig. 5 (c) corroborates that the equiaxed grains have an average size of 7.6 µm, while the columnar grains almost double in size the equiaxed ones with an average value of 13.4 µm. These figures show that the largest grain size growths are located in the central part of the MPs. On the other hand, higher concentrations of smaller grains can be found at the MPs' extremes. This behavior confirms thermal gradients' formation, which mainly affects the central zone of the MPs, where the next layer melts and radiates heat towards the extremes. According to [25], elongated grains are produced and oriented in the thermal gradient direction.

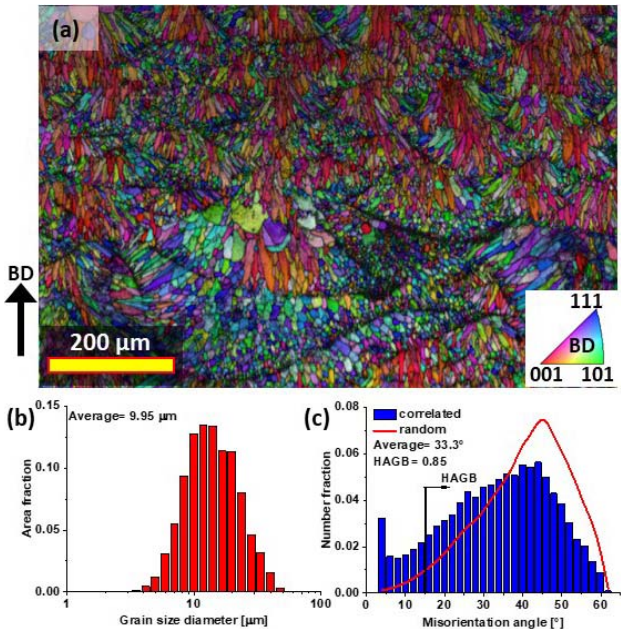

Fig. 4 (a) IPF map, (b) grain size distribution, and (c) misorientation angle distribution

Analyzing the texture for the two families of grains, Fig. 5 (d) indicates through pole figures (PF) that the columnar grains' texture is dominated by the presence of Cube and Goss type components. Additionally, the grains with equiaxed

morphology and smaller size show a texture with a high intensity of the Goss component. For this reason, the FP of all grains indicates a clear dominance of the Goss component. According to various investigations [26]-[28] in Al alloys, components such as Goss and Cubo are linked with recrystallization phenomena in the material. Thus, the formation of small and big grains can be attributed to two recrystallization phenomena—the first, larger initial grains give rise to smaller recrystallized grains. Second, larger grains are associated with recrystallization at higher temperatures, leading to abrupt grain growth (i.e., columnar grains).

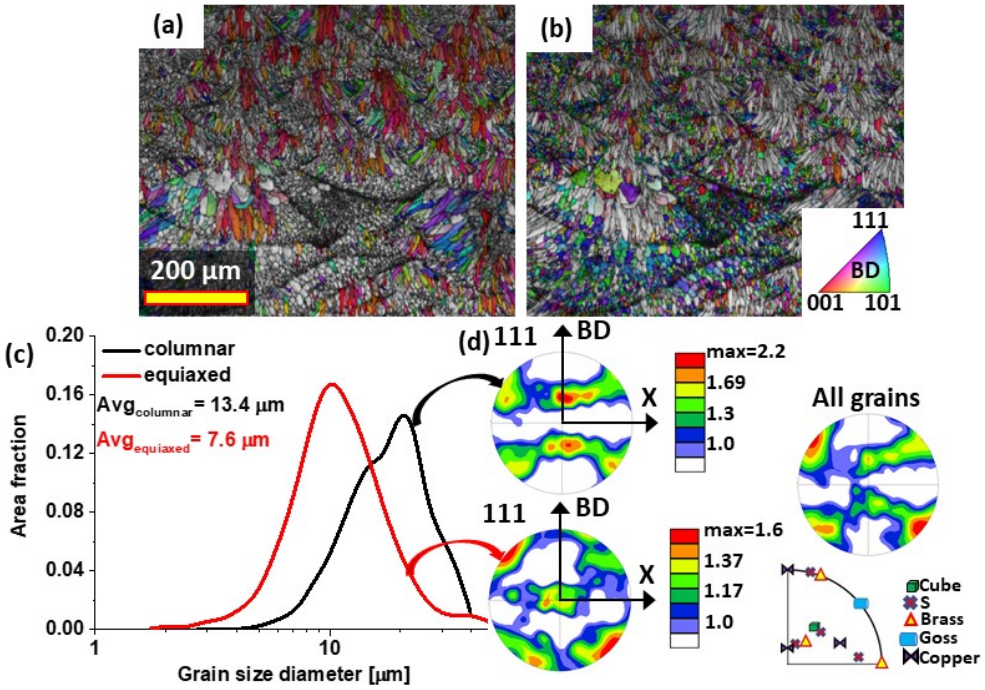

Fig. 5 (a) columnar grains IPF map, (b) equiaxed grains IPF map, (c) columnar and equiaxed grains size distribution, and (d) PFs for columnar and equiaxed grains

D.Mechanical Properties

Fig. 6 indicates the tensile mechanical properties of the printed alloy. Its values are compared with those obtained by casting processes and a combination of conventional deformation processes with severe plastic deformation [29]. At first glance, the printed alloy strength and ductility values change depending on the direction; e.g., the radial direction, where the MPs are oriented perpendicular to the load direction, presented the best strength and ductility values. On the contrary, the longitudinal direction, where the melt pools are parallel to the load direction, has the worst performance. Therefore, it can be inferred that the preferential orientation of the columnar grains in the BD can act as a failure mechanism, either transgranular or through the MPBs. However, it is worth mentioning that much higher strengths can be achieved for the same alloy through AM processes than by using casting and grain refinement through severe plastic deformation techniques. In this way, the great potential of AM technologies to give way to a new generation of materials is verified. The fact that high solidification and cooling rates are involved in SLM makes it possible to obtain heterogeneous microstructures with different characteristics to those obtained with traditional processes. However, further studies are still required to improve the strain hardening capacity of printed materials.

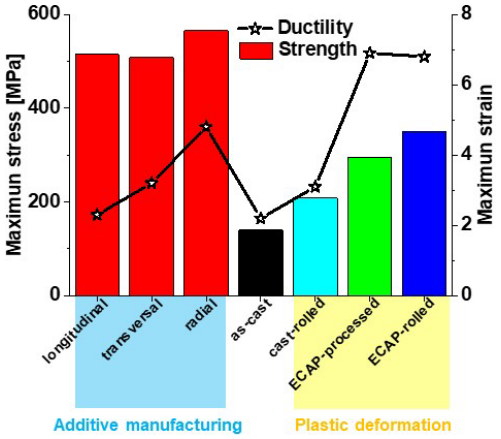

Fig. 6 Mechanical properties summary

IV. Conclusion

Through AM, using the SLM process, an AlSi11Cu alloy was successfully printed. The alloy indicated a structure formed by an Al matrix surrounded by a network enriched in Si. The manufacturing process generated a heterogeneous

microstructure formed by small and equiaxed grains and larger grains with columnar morphology. Additionally, the texture studies demonstrated the dominance of recrystallization components such as Goss and Cubo, indicating the nucleation of new grains and other grains' abnormal growth. In this way, the microstructure's heterogeneity helped obtain variations in the alloy's strength, depending on the direction of measurement concerning the BD. It was also shown that the mechanical properties obtained for this type of alloys are superior to those obtained by processes such as casting and severe plastic deformation.

ACKNOWLEDGMENT

The authors gratefully acknowledge the financial support of the Ministry of Science and Higher Education of the Russian Federation in the framework of Increase Competitiveness Program of NUST «MISiS» (№ К4-2019-045), implemented by a governmental decree dated 16th of March 2013, N 211. The authors also acknowledge the financial support of the Russian Science Foundation (RSF) (grant № 19-79-30025).

CONFLICT OF INTEREST

The authors declare no conflict of interest.

REFERENCES

[1] J. Podroužek, M. Marcon, K. Ninčević, R. Wan-Wendner, Bio-Inspired 3D Infill Patterns for Additive Manufacturing and Structural Applications, Materials (Basel). 12 (2019). doi:10.3390/ma12030499.

[2] A. Paolini, S. Kollmannsberger, E. Rank, Additive manufacturing in construction: A review on processes, applications, and digital planning methods, Addit. Manuf. 30 (2019) 100894. doi: https://doi.org/10.1016/j.addma.2019.100894.

[3] D. Delgado Camacho, P. Clayton, W.J. O'Brien, C. Seepersad, M. Juenger, R. Ferron, S. Salamone, Applications of additive manufacturing in the construction industry – A forward-looking review, Autom. Constr. 89 (2018) 110–119. doi:https://doi.org/10.1016/j.autcon.2017.12.031.

[4] T.D. Ngo, A. Kashani, G. Imbalzano, K.T.Q. Nguyen, D. Hui, Additive manufacturing (3D printing): A review of materials, methods, applications and challenges, Compos. Part B Eng. 143 (2018) 172–196. doi: https://doi.org/10.1016/j.compositesb.2018.02.012.

[5] M. Attaran, The rise of 3-D printing: The advantages of additive manufacturing over traditional manufacturing, Bus. Horiz. 60 (2017) 677–688. doi:https://doi.org/10.1016/j.bushor.2017.05.011.

[6] J. Jiang, X. Xu, J. Stringer, Support Structures for Additive Manufacturing: A Review, J. Manuf. Mater. Process. 2 (2018). doi: 10.3390/jmmp2040064.

[7] C.Y. Yap, C.K. Chua, Z.L. Dong, Z.H. Liu, D.Q. Zhang, L.E. Loh, S.L. Sing, Review of selective laser melting: Materials and applications, Appl. Phys. Rev. 2 (2015) 41101. doi:10.1063/1.4935926.

[8] W.S.W. Harun, K. Kadirgama, M. Samykano, D. Ramasamy, I. Ahmad, M. Moradi, 5 - Mechanical behavior of selective laser melting-produced metallic biomaterials, in: J.P. Davim (Ed.), Mech. Behav. Biomater., Woodhead Publishing, 2019: pp. 101–116. doi: https://doi.org/10.1016/B978-0-08-102174-3.00005-X.

[9] W. Gao, Y. Zhang, D. Ramanujan, K. Ramani, Y. Chen, C.B. Williams, C.C.L. Wang, Y.C. Shin, S. Zhang, P.D. Zavattieri, The status, challenges, and future of additive manufacturing in engineering, Comput. Des. 69 (2015) 65–89. doi: https://doi.org/10.1016/j.cad.2015.04.001.

[10] S. Singh, S. Ramakrishna, R. Singh, Material issues in additive manufacturing: A review, J. Manuf. Process. 25 (2017) 185–200. doi: https://doi.org/10.1016/j.jmapro.2016.11.006.

[11] N.T. Aboulkhair, M. Simonelli, L. Parry, I. Ashcroft, C. Tuck, R. Hague, 3D printing of Aluminium alloys: Additive Manufacturing of Aluminium alloys using selective laser melting, Prog. Mater. Sci. 106 (2019) 100578. doi: https://doi.org/10.1016/j.pmatsci.2019.100578.

[12] H. Zhang, H. Zhu, T. Qi, Z. Hu, X. Zeng, Selective laser melting of high strength Al–Cu–Mg alloys: Processing, microstructure and mechanical properties, Mater. Sci. Eng. A. 656 (2016) 47–54. doi: https://doi.org/10.1016/j.msea.2015.12.101.

[13] N. Kaufmann, M. Imran, T.M. Wischeropp, C. Emmelmann, S. Siddique, F. Walther, Influence of Process Parameters on the Quality of Aluminium Alloy EN AW 7075 Using Selective Laser Melting (SLM), Phys. Procedia. 83 (2016) 918–926. doi: https://doi.org/10.1016/j.phpro.2016.08.096.

[14] A. Aversa, G. Marchese, A. Saboori, E. Bassini, D. Manfredi, S. Biamino, D. Ugues, P. Fino, M. Lombardi, New Aluminum Alloys Specifically Designed for Laser Powder Bed Fusion: A Review, Materials (Basel). 12 (2019). doi: 10.3390/ma12071007.

[15] F. Trevisan, F. Calignano, M. Lorusso, J. Pakkanen, A. Aversa, E.P. Ambrosio, M. Lombardi, P. Fino, D. Manfredi, On the Selective Laser Melting (SLM) of the AlSi10Mg Alloy: Process, Microstructure, and Mechanical Properties, Materials (Basel). 10 (2017). doi: 10.3390/ma10010076.

[16] X. Liu, C. Zhao, X. Zhou, Z. Shen, W. Liu, Microstructure of selective laser melted AlSi10Mg alloy, Mater. Des. 168 (2019) 107677. doi: https://doi.org/10.1016/j.matdes.2019.107677.

[17] F. Yan, W. Xiong, E.J. Faierson, Grain Structure Control of Additively Manufactured Metallic Materials, Materials (Basel). 10 (2017). doi: 10.3390/ma10111260.

[18] Y. Zhu, X. Tian, J. Li, H. Wang, The anisotropy of laser melting deposition additive manufacturing Ti–6.5Al–3.5Mo–1.5Zr–0.3Si titanium alloy, Mater. Des. 67 (2015) 538–542. doi: https://doi.org/10.1016/j.matdes.2014.11.001.

[19] L. Hitzler, J. Hirsch, B. Heine, M. Merkel, W. Hall, A. Öchsner, On the Anisotropic Mechanical Properties of Selective Laser-Melted Stainless Steel, Materials (Basel). 10 (2017). doi: 10.3390/ma10101136.

[20] Y. Kok, X.P. Tan, P. Wang, M.L.S. Nai, N.H. Loh, E. Liu, S.B. Tor, Anisotropy and heterogeneity of microstructure and mechanical properties in metal additive manufacturing: A critical review, Mater. Des. 139 (2018) 565–586. doi: https://doi.org/10.1016/j.matdes.2017.11.021.

[21] I. Rosenthal, A. Stern, N. Frage, Microstructure and Mechanical Properties of AlSi10Mg Parts Produced by the Laser Beam Additive Manufacturing (AM) Technology, Metallogr. Microstruct. Anal. 3 (2014) 448–453. doi:10.1007/s13632-014-0168-y.

[22] Y.J. Liu, Z. Liu, Y. Jiang, G.W. Wang, Y. Yang, L.C. Zhang, Gradient in microstructure and mechanical property of selective laser melted AlSi10Mg, J. Alloys Compd. 735 (2018) 1414–1421. doi: https://doi.org/10.1016/j.jallcom.2017.11.020.

[23] J. Wu, X.Q. Wang, W. Wang, M.M. Attallah, M.H. Loretto, Microstructure and strength of selectively laser melted AlSi10Mg, Acta Mater. 117 (2016) 311–320. doi: https://doi.org/10.1016/j.actamat.2016.07.012.

[24] U. Tradowsky, J. White, R.M. Ward, N. Read, W. Reimers, M.M. Attallah, Selective laser melting of AlSi10Mg: Influence of post-processing on the microstructural and tensile properties development, Mater. Des. 105 (2016) 212–222. doi: https://doi.org/10.1016/j.matdes.2016.05.066.

[25] N.T. Aboulkhair, N.M. Everitt, I. Ashcroft, C. Tuck, Reducing porosity in AlSi10Mg parts processed by selective laser melting, Addit. Manuf. 1–4 (2014) 77–86. doi: https://doi.org/10.1016/j.addma.2014.08.001.

[26] J. Alberto Muñoz, A. Komissarov, M. Avalos, R.E. Bolmaro, Heat treatment effect on an AA6063 alloy, Mater. Lett. 277 (2020) 128338. doi: https://doi.org/10.1016/j.matlet.2020.128338.

[27] J.A. Muñoz, O.F. Higuera, V. Tartalini, P. Risso, M. Avalos, R.E. Bolmaro, Equal channel angular sheet extrusion (ECASE) as a precursor of heterogeneity in an AA6063-T6 alloy, Int. J. Adv. Manuf. Technol. 102 (2019) 3459–3471. doi: 10.1007/s00170-019-03425-7.

[28] J.A. Muñoz, M. Avalos, R.E. Bolmaro, Heterogeneity of strain path, texture and microstructure evolution of AA6063-T6 processed by Equal Channel Angular Sheet Extrusion (ECASE), J. Alloys Compd. 768 (2018) 349–357. doi: 10.1016/j.jallcom.2018.07.216.

[29] D. Song, G. Wang, Z. Zhou, E.E. Klu, B. Gao, A. Ma, Y. Wu, J. Sun, J. Jiang, X. Ma, Developing a high-strength Al–11Si alloy with improved ductility by combining ECAP and cryorolling, Mater. Sci. Eng. A. 773 (2020) 138880. doi: 10.1016/j.msea.2019.138880.